Tracking the magnetic field in the Fermilab Muon g-2 experiment

René Reimann[∗] **for the Muon g-2 collaboration**

Institute of Physics & PRISMA+ Cluster of Excellence, Johannes Gutenberg University Mainz, Staudinger Weg 7, 55099 Mainz, Germany

E-mail: rreimann@uni-mainz.de

Recently the Muon g-2 collaboration published the most precise measurement of the anomalous magnetic moment of the muon, a_μ, with a 460 ppb uncertainty based on the Run-1 data. The measurement principle is based on a clock comparison between the anomalous spin precession frequency of spin-polarized muons and a high-precision measurement of the magnetic field environment using nuclear magnetic resonance (NMR) techniques, expressed by the shielded proton spin precession frequency. To achieve the ultimate goal of a 140 ppb uncertainty on a_μ, the magnetic field in the storage region of the muons needs to be known with a total uncertainty of less than 70 ppb. Three devices are used to measure and calibrate the magnetic field in the Muon g-2 storage ring: (a) an absolute-calibrated NMR probe, (b) a movable array of NMR probes that can be pulled through the storage region of the muons and (c) a set of NMR probes outside of the vacuum chambers surrounding the storage region. Here we present the measurement and tracking principle of the magnetic field and point out improvements implemented for the analysis of the data recorded during Run-2 and Run-3.

[∗]Speaker

1. The magnetic moment of the muon

The muon g factor, g_μ, relates the spin of the muon, $\vec{S}$, to its magnetic moment, $\vec{\mu}_\mu = -g_\mu \frac{e}{2m_\mu} \vec{S}$. At tree level, the magnetic moment of a spin 1/2 particle is $g = 2$ [1] and higher order corrections are expressed by the anomalous magnetic moment of the muon $a_\mu = \frac{g-2}{2}$.

Muons stored in a homogeneous magnetic field undergo cyclotron motion with angular frequency $\vec{\omega}_c$ and due to their magnetic moment also their spin precesses with a frequency $\vec{\omega}_a$. The Fermilab Muon g-2 experiment measures the anomalous spin precession frequency $\vec{\omega}_a = \vec{\omega}_s - \vec{\omega}_c = -a_\mu \frac{q}{m_\mu} \vec{B}$ by observing positrons e^+ from decays of muon stored in the storage ring magnet. The decay positron emission direction in the muons' rest frame depends on the muons' spin orientation, which is observed in the laboratory frame as an energy modulation with ω_a. Using nuclear magnetic resonance (NMR) techniques, the magnetic field is measured in terms of the spin precession frequency of protons $\omega'_p(T)$ in an ultra pure water sample at temperature T using ratios of quantities measured to high precision. By this a_μ can be determined by

$$a_\mu = \frac{\omega_a}{\tilde{\omega}'_p} \cdot \frac{\mu'_p}{\mu_e(H)} \frac{\mu_e(H)}{\mu_e} \frac{m_\mu}{m_e} \frac{g_e}{2} \tag{1}$$

where the Muon g-2 experiment measures the ratio $\frac{\omega_a}{\tilde{\omega}'_p}$ and where $\tilde{\omega}'_p$ corresponds to the magnetic field experienced by the muons. Here $\frac{\mu'_p}{\mu_e(H)}$ is the shielded proton-to-electron magnetic moment ratio [2], g_e is the electron g-factor [3], $\frac{m_\mu}{m_e}$ is the muon-to-electron mass ratio [4, 5], and $\mu_e(H)/\mu_e$ is a QED factor computed by theory with negligible uncertainty [4]. These external high precision measurements contribute a total uncertainty of 25 ppb on a_μ.

The Fermilab Muon g-2 collaboration measured $a_{\mu,\text{FNAL}} = 116\,592\,040(54) \times 10^{-11}$ [6] in Run-1 using data from 2018, which is in good agreement with the result from BNL E821 [7]. The combined experimental world average shows a $4.2\,\sigma$ tension with the standard model prediction using a dispersive approach to extract the hadronic vacuum polarisation component from e^+e^- cross-section measurements [8]. Recent lattice QCD calculations evaluated the QCD terms, which are the dominant uncertainties in the theory calculations. These evaluations reduce the discrepancy with the experimental value to $1.5\,\sigma$ [9] and show a discrepancy of $2.2\,\sigma$ between the two calculation methods. Currently the Fermilab Muon g-2 experiment has recorded data from Run-2 to Run-5 and is analysing the data of Run-2 and Run-3.

The measured raw frequencies need to be corrected for various systematic effects:

$$\frac{\omega_a}{\tilde{\omega}'_p} \approx \frac{f_{\text{clock}} \omega_a^{\text{meas}}(1 + C_e + C_p + C_{ml} + C_{pa})}{f_{\text{calib}}\langle M(x,y,\phi)\omega'_p(x,y,\phi)\rangle(1 + B_k + B_q)} \,. \tag{2}$$

The determination of ω_a^{meas} is described in [10, 11] and the correction terms C_e, C_p, C_{ml} and C_{pa}, caused by beam dynamic effects, are described in [12–14]. Here we discuss the tracking of the magnetic field on time scales from seconds up to several days, based on the proton spin-precession frequency $\omega'_p(x,y,\phi)$[1], the muon beam profile $M(x,y,\phi)$, the calibration of the measurement probes f_{calib} and correction factors due to transient magnetic fields B_k and B_q. We point out improvements compared to the Run-1 analysis, described in [15].

---

[1]x, y and ϕ are position coordinates in the Muon g-2 storage region.

2. The 1.45T storage ring magnet

The magnetic field is provided by a superconducting storage ring magnet that was recycled from the Brookhaven Muon g-2 experiment [16]. The storage ring magnet is designed for muons at the magic momentum $p_\mu^{\text{magic}} = 3.094\frac{\text{GeV}}{c} \pm 0.5\%$ and provides a 1.45 T vertical magnetic field. The muon storage region is 90 mm in diameter at a nominal radius of 7.112 m. Between the poles of the magnet a 180 mm gap allows for the installation of vacuum chambers. The magnet was shimmed passively by metal shim pieces and metal foils. Drift is actively stabilized by a power supply feedback based on field measurements around the ring. 100 surface coils are installed in both the top and bottom pole pieces, allowing for correction of azimuthally averaged residual gradients.

Figure 1: Cross-section of superconducting storage ring magnet [6].

At one location in the ring, a superconducting inflector magnet cancels the field in the return yoke to allow the incoming muon beam to enter the storage ring volume. A superconducting shield freezes the magnetic field in storage region prior to ramp up of the inflector magnet.

3. Tracking the magnetic field

The magnetic field in the storage ring volume is measured by NMR probes that use petroleum jelly as active proton-rich sample. The spins of the protons are rotated out of equilibrium by applying a RF $\pi/2$-pulse perpendicular to the external magnetic field by a coil. The resulting spin precession induces a small current in the excitation coil which is digitized. Using a Hilbert transform, the phase and amplitude of the signal are extracted and the frequency difference is measured by comparing to a phase template from the same probe [17].

The magnetic field is measured with three systems. The first system is a moving measurement device, called the trolley, which houses 17 NMR probes. The trolley is pulled through the ring on rails every 3-5 days, measuring the spatial field distribution in the storage region at > 8000 azimuthal locations [18]. Compared to Run-1 the position determination based on a barcode on the face of the vacuum chambers was improved.

The second system consists of 378 NMR probes which are located in the walls of the vacuum chambers, tracking the field drift continuously. The probes are located at 72 azimuthal locations, called stations, with either four or six probes each.

The measured magnetic field is expressed by multipole coefficients which are given by

$$B(r, \theta) = B_0 + \sum_{n=1}^{4} \left(\frac{r}{r_0}\right)^n \left[a_n \cos(n\theta) + b_n \sin(n\theta)\right] \tag{3}$$

where B_0 is the dipole moment (the constant magnetic field) and a_n, b_n are the coefficients of gradients of order n. While the trolley measures up to 17 multipole moments, a fixed probe station can extract either 4 or 5 multipole moments.

To track the magnetic field, the measurements from a trolley run are synchronized with the fixed probe system, so that the magnetic field drift can be corrected for times in between two trolley
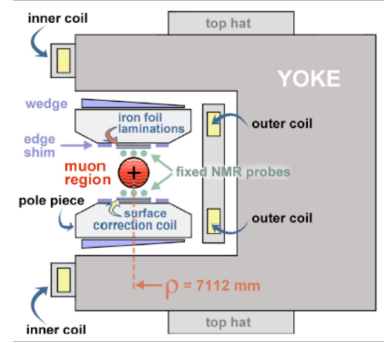
runs. The synchronization of the systems requires to remove the trolley footprint caused by material effects of the trolley itself, which is clearly visible in the fixed probes when the trolley passes by. The measurements around that time are vetoed and interpolated from neighbouring probes.

Using the magnetic field at a first trolley run and the drift correction from the fixed probes, the magnetic field at the time of a second trolley run can be predicted and compared to the actually measured values. The difference, called tracking offset, describes the limitations of the tracking method. The tracking offset is expected to follow a random walk. For the final magnetic field value the drift is additionally corrected by a linear slope so that both trolley runs are matched exactly. The residual uncertainties relative to the linear interpolation can be described by a Brownian bridge model.

Compared to Run-1, the azimuth is treated continuously instead of station-wise

Figure 2: Azimuthal averaged magnetic field map (contour lines) and beam profile (colorbar) [6].

in the tracking analysis. The synchronization using the trolley footprint and interpolation was refined. More trolley runs allow for a better understanding of the tracking offset, which would average out if they are uncorrelated and unbiased. Better temperature regulation, magnet insulation with blankets and improved AC system of the experimental hall lead to improved field stability and tracking drifts become smaller and thus lead to less uncertainty.

The final step in the analysis is the convolution of the magnetic field distribution with the muon beam profile so that $\tilde{\omega}'_p$ corresponds to the magnetic field as seen by the muons. The muon beam profile is based on positron tracker profiles [19] which are measured at two locations in the ring and beam dynamic simulations to translate these measurements to other azimuthal locations. The convolution is done by taking the product of the multipole expansion of the magnetic field and the multipole expansion of the muon beam profile. The azimuthally averaged muon profile and magnetic field from Run-1 is shown in Fig. 2.

Improved running conditions, e.g. replacement of broken resistors in the electrostatic quadrupoles and a stronger kick lead to better placement of the beam on the nominal storage orbit, reducing uncertainties caused by the asymmetric beam profile in Run-1.

4. Absolute field calibration

The trolley NMR probes are filled with petroleum jelly and need to be calibrated with an ultra pure water sample. Therefore, an absolute-calibrated probe with ultra pure water, which was cross-calibrated at Argonne National Laboratory test magnet [20], is used. For calibration the absolute-calibrated probe is mounted onto a 3D translation stage and the same position is repeatedly measured with a trolley probe and the absolute-calibrated probe. Careful alignment and fine shimming are key for a precise calibration for each trolley probe. Correction factors to
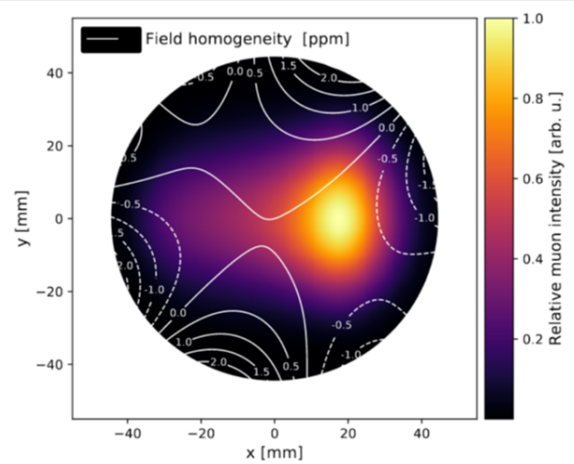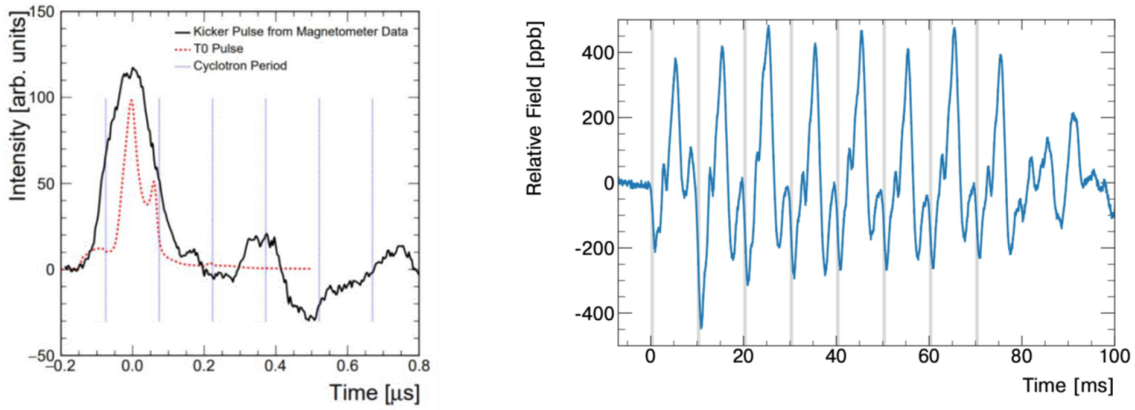
Figure 3: Left: Magnetic field as function of time while a kicker pulse. Right: Magnetic field measured inside an electrostatic quadrupole on the time scale of eight muon bunches (gray bands) [6].

relate the absolute-calibrated probe for protons in a spherical water sample at 34.7°C are calculated. The probe was cross-calibrated to the absolute-calibrated probe used in the J-PARC Muon g-2 experiment. Further the calibration was confirmed by hyperpolarized He3 [21].

The calibration is performed twice a year with automated procedures which lead to very consistent results. In addition temperature effects are studied in detail.

5. Transient magnetic fields

During the first revolution, the muon beam has to be placed onto its nominal storage orbit. This is achieved by a kicker pulse [22] that induces a 22 mT vertical field within the first revolution (~140 ns). The fixed probes system runs asynchronously to the beam injection and fast magnetic field changes are shielded by the aluminium of the vacuum chambers. Specialized measurements were taken using a magnetometer based on optical Faraday rotation using a terbium gallium garnet crystal and optical fiber to bring laser light into the measurement device. By measuring the difference between the two light polarizations the fast kicker transient can be measured (see Fig. 3 left). Compared to Run-1, additional data were taken with reduced uncertainties due to vibration mitigation that have been the limiting noise contribution in the first measurement campaign. A second independent magnetometer without fibers took data in July 2022.

To keep the muon beam stored, electrostatic quadrupoles occupy about 43% of the ring [23]. They are quasi-static on the time scale the muons are present but are pulsed between muon bunches to clear the volume from trapped particles in the quasi Penning trap which is created by the magnetic field and the electric field of the quadrupoles. The pulsing leads to magnetic transient fields which introduce mechanical vibrations of the quadrupole plates which in turn disturbs the magnetic field. Again the fast transient magnetic field is shielded by the aluminium of the vacuum walls such that the fixed probe system only sees a very weak signal. Special NMR probes with a housing made out of polyether ether ketone (PEEK) are used to measure these transient fields. These measurements were done after Run-2 only at a few places around the ring, thus in Run-1 a conservative estimate of this effect was used. A full mapping campaign of the storage ring has taken place between Run-4 and Run-5 showing a very reproducible pattern.

6. Summary / Conclusions

With the measurement of the anomalous magnetic moment and the theoretical prediction based on a dispersive approach and based on lattice QCD calculations, a three way comparison is possible for the first time. The Fermilab Muon g-2 experiment published the result of Run-1, while Run-2/3 analysis is on-going and data taking of Run-4/5 is completed. The precise determination of the magnetic field seen by the muons in the storage ring magnet is done with three systems based on NMR techniques. The trolley system measures the spatial distribution while the fixed probe system tracks the magnetic field drift over time. The field is calibrated using an absolute-calibrated ultra-pure water probe twice a year. Detailed measurement campaigns are performed to measure transient magnetic fields from kicker and electrostatic quadrupoles.

Improved running conditions (e.g. temperature stability), data processing (e.g. position reconstruction and frequency extraction) and analysis as well as additional systematic studies will lead to reduced systematic uncertainties in the upcoming results together with improved statistics.

References

[1] P. A. M. Dirac, Proceedings of the Royal Society of London. Series A **117**, 610 (1928).

[2] W. D. Phillips *et al.*, Metrologia **13**, 179 (1977).

[3] D. Hanneke *et al.*, Physical Review A **83**, 052122 (2011).

[4] E. Tiesinga *et al.*, "The 2018 CODATA recommended values of the fundamental physical constants (Web Version 8.1)," https://physics.nist.gov/cuu/Constants/ (2018).

[5] W. Liu *et al.*, Physical Review Letters **82**, 711 (1999).

[6] The Muon g-2 Collaboration, B. Abi, *et al.*, Physical Review Letters **126**, 141801 (2021).

[7] G. W. Bennett *et al.*, Physical Review D **73**, 072003 (2006).

[8] T. Aoyama *et al.*, Physics Reports **887**, 1 (2020).

[9] S. Borsanyi *et al.*, Nature **593**, 51 (2021).

[10] L. Cotrozzi and M. Sorbara (Muon g-2), PoS(ICHEP2022) , 749 (2022), these proceedings.

[11] The Muon g-2 Collaboration, T. Albahri, *et al.*, Physical Review D **103**, 072002 (2021).

[12] P. Girotti (Muon g-2), PoS(ICHEP2022) , 228 (2022), these proceedings.

[13] A. Driutti (Muon g-2), PoS(ICHEP2022) , 053 (2022), these proceedings.

[14] The Muon g-2 Collaboration, T. Albahri, *et al.*, Physical Review Accelerators and Beams **24**, 044002 (2021).

[15] The Muon g-2 Collaboration, T. Albahri, *et al.*, Physical Review A **103**, 042208 (2021).

[16] G. T. Danby *et al.*, Nuclear Instruments and Methods in Physics Research Section A **457**, 151 (2001).

[17] R. Hong *et al.*, Journal of Magnetic Resonance **329**, 107020 (2021).

[18] S. Corrodi *et al.*, Journal of Instrumentation **15**, P11008 (2020).

[19] B. T. King *et al.*, Journal of Instrumentation **17**, P02035 (2022).

[20] D. Flay *et al.*, Journal of Instrumentation **16**, P12041 (2021).

[21] M. Farooq *et al.*, Physical Review Letters **124**, 223001 (2020).

[22] A. P. Schreckenberger *et al.*, Nuclear Instruments and Methods in Physics Research Section A **1011**, 165597 (2021).

[23] Y. K. Semertzidis *et al.*, Nuclear Instruments and Methods in Physics Research Section A **503**, 458 (2003).